A PARETO-OPTIMAL APPROACH TO MULTI-MATERIAL TOPOLOGY OPTIMIZATION

Amir M. Mirzendehdel
Department of Mechanical Engineering
UW-Madison
Madison, Wisconsin 53706, USA
Email: mirzendehdel@wisc.edu

Krishnan Suresh
Department of Mechanical Engineering
UW-Madison
Madison, Wisconsin 53706, USA
Email: ksuresh@wisc.edu

ABSTRACT

As additive manufacturing expands into multi-material, there is a demand for efficient multi-material topology optimization, where one must simultaneously optimize the topology, and the distribution of various materials within the topology.

The classic approach to multi-material optimization is to minimize compliance or stress while imposing two sets of constraints: (1) a total volume constraint, and (2) individual volume-fraction constraint on each of the material constituents. The latter can artificially restrict the design space. Instead, the total mass and compliance are treated as conflicting objectives, and the corresponding Pareto curve is traced; no additional constraint is imposed on the material composition.

To trace the Pareto curve, first order element sensitivity fields are computed, and a two-step algorithm is proposed. The effectiveness of the algorithm is demonstrated through illustrative examples in 3D.

Keywords Topology optimization, Multi-material structures, Pareto tracing, matrix-free FEA.

1. INTRODUCTION

Topology optimization (TO) [1], [2], [3] is exploited today to optimize aircraft components [4], [5], spacecraft modules [6], automobiles components [7], and compliant mechanisms [8]–[11]. It strongly complements the growing field of additive manufacturing (AM) in that the complex designs created through the former can, in theory, be directly fabricated through AM. The optimality of the design created through TO ensures that the least amount of material is used, translating into reduced fabrication time and material cost (see Figure 1). This serves as a primary motivation for this paper.

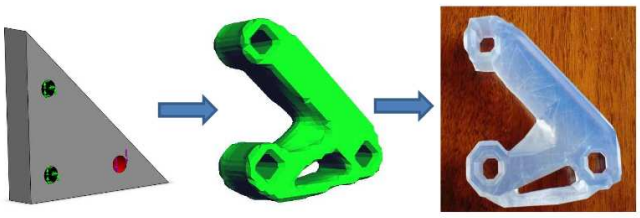

Figure 1: From problem specification to optimal part.

However, there are a number of practical issues that need to be addressed [12]. These issues include AM-specific TO, design of support structures, minimum feature size, accounting for material de-bonding, accounting for residual stresses, etc.

With new technological innovations in AM, new challenges arise in TO. For instance, AM can now support multiple materials, i.e., one can now control the material composition, and internal structural pattern with sub-millimeter precision. For example, the OpenFab project from MIT [13] discusses a programmable pipeline for synthesis of multi-material 3D printed objects. The key feature in this pipeline is the voxelization of the object.

This creates a strong need for high-resolution multi-material topology optimization (MMTO), where one must simultaneously optimize the topology and the distribution of various materials within a given space. While MMTO has been addressed by researchers for over two decades now [14], the objective of this paper is to pursue a MMTO method that is computationally efficient and can be generalized to variety of objectives.

In Section 2, recent advances in MMTO are summarized. In Section 3, we propose an efficient MMTO method that generalizes the single-material Pareto-tracing method proposed in [15], [16]. In Section 4, the validity of this method is confirmed through benchmark case-studies. Section 5 summarizes the contributions of this paper.

2. LITERATURE REVIEW

In this section we briefly review technical background on single-material topology optimization (SMTO), and then discuss recent research on multi-material topology optimization (MMTO).

2.1 Single Material Topology Optimization

Classic SMTO problems may be posed as:

$$\begin{aligned} &\underset{\Omega \subset D}{Min}\ \varphi \\ &g_i(u,\Omega) \le 0 \\ &\text{subject to} \\ &Ku = f \end{aligned} \tag{1}$$

where:

φ : Objective such as compliance,stress, or volume
Ω : Topology to be computed
D : Domain within which the topology must lie
u : Finite element displacement vector
K : Finite element stiffness matrix
f : External force vector
g_i : Constraints on volume, stress, buckling, ...

In other words, the objective is to find the optimal design, within a given design space, that minimizes a specific objective and satisfies certain design constraints. Typical objectives include volume fraction, compliance, etc., while constraints include displacement, stress, buckling, and manufacturing constraints. A typical structural problem is illustrated in Figure 2, where the thickness of the structure is 5 units, and the load is 100 units.

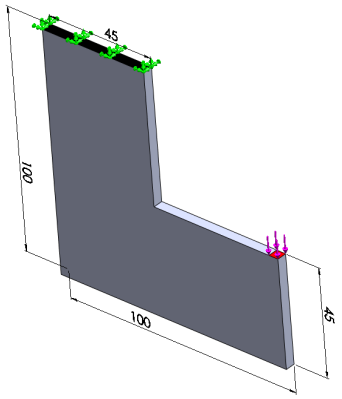

Figure 2: Design space for a topology optimization problem.

Various topology optimization methods such as homogenization [17], Solid Isotropic Material with Penalization (SIMP) [18], level-set [19]–[22], and evolutionary methods [23]–[25], have been proposed for solving such problems; please see [26], [27] for recent reviews.

The key concept in SIMP is to describe the material distribution by a pseudo-density variable ρ that interpolates the underlying material properties [24]; for example, the Young's modulus is typically interpolated per element via:

$$E_e = \rho_e^p E_0 \tag{2}$$

The penalization factor p depends on the physics and dimension of the problem; it is typically assigned a value of '3' for 3D linear elasticity. The pseudo-density variables are then optimized to reach the desired objective. For the problem posed in Figure 2, any of the above methods can be used for finding the optimal topology. Variations of this concept include node-based SIMP [28] and multi-resolution SIMP [29].

2.2 Multi-Material Topology Optimization

For multi-material topology optimization (MMTO), the problem posed in Equation (1) is generalized to:

$$\begin{aligned} &\underset{\Omega_{k=1,2..M} \subset D}{Min}\ \varphi \\ &\Omega_i \cap \Omega_{j \neq i} = \varnothing \\ &g_i(u, \Omega_k) \leq 0 \\ &\text{subject to} \\ &Ku = f \end{aligned} \tag{3}$$

where (also see Equation (1)):

$$\begin{aligned} &\Omega_k: \text{ Topology for material '}k\text{' to be computed} \\ &M: \text{ Number of materials} \end{aligned}$$

Thus the objective is to find the optimal distribution of M non-overlapping materials, within a given design space, that minimizes a specific objective and satisfies certain design constraints.

The MMTO problem posed in Equation (3) assumes that every point within the design space has a distinct material associated with it (or is void). This differs from functionally graded material optimization [30], where a mixture of base materials is allowed.

SIMP-Based MMTO. For multiple materials, the SIMP approach was first extended to multiple materials in 1992 [14]. However, the challenges associated with assigning different interpolations for different materials and material properties was discussed in [31] where Sigmund proposed a two-material interpolation scheme for designing thermally and electro-thermally driven micro actuators. An alternate material interpolation strategy was developed in [32] by introducing a peak function and exploiting optimality criteria method.

A new SIMP method was presented in [33] for optimizing multiple homogeneous materials, which interpolates the stiffness matrix instead of interpolating the Young's modulus. The validity of this method was demonstrated through 2D examples involving two materials. In [34], Chavez et al. implemented SIMP to solve a special problem of minimizing the compliance of concrete slabs reinforced with carbon fibers. Their approach relies on concrete failure criteria, and the fact that the slabs are simple symmetric geometries in 2D. In 2007, De Kruijf et al. employed SIMP to minimize both compliance and resistance to heat dissipation of composites. The method is in 2D and attains only the upper limits of Hashin-Shtrikman [35]. If the materials are composites, it is well-known that SIMP interpolations can violate Hashin-Shtrikman bounds [27]. Blasques and Stolpe proposed a density-based framework for minimizing compliance of laminated composite beam cross sections [36]. The method allows multi-material laminates in 2D, where the formulation is carried out by writing equilibrium between laminate layers, under the limiting assumptions that the beam is slender and has invariant cross sections.

A new multi-resolution scheme for MMTO was developed in [37] where different levels of discretization were employed for representing displacement, design variables, and density. The method uses the alternating active phase algorithm, in which the original problem is decomposed into a number of sub-problems, where only two of the materials are active, and the problem is solved using the density approach.

Level-Set and Phase-Field MMTO. In 2003, Wang and Wang introduced a novel level-set approach for MMTO [38]. The method requires M level-sets to represent 2^M distinct materials, and it was used to solve benchmark problems in 2D, where different 'colored level-sets' represented distinct materials.

Later, the idea was expanded towards compliant mechanism design [39] and microstructures [40]. Unfortunately, as demonstrated in [41], these shape derivatives were approximations under certain assumptions. Allaire et al. developed the correct mathematical shape derivatives in [41] where the interface zone thickness is also kept constant. In order to remove discontinuity caused by sharp interfaces, authors of [42] suggested using multiple intermediate interfaces to attain continuity. The most challenging issues in MMTO via level-set are: (1) field discontinuity, and (2) thickness diffusion. The former is due to discontinuity in phase properties, which leads to discontinuous normal strain and tangential stress. The latter is caused by numerical diffusion in level-set process [41].

Wang and Zhou [43] presented the phase-field method for MMTO using Van der Waals–Cahn-Hilliard theory for dynamic phase transition. The method makes no distinction between the material phases and their interface.

More recently, as an improvement over the idea proposed in [38], a new multi-material level-set method was proposed in [44] for

both shape and topology optimization. While exact sensitivity expression were provided, the implementation was restricted to 2D.

Evolutionary Methods for MMTO. Yet another family of topology optimization methods are the evolutionary-based methods. Xie and Steven, first developed evolutionary structural optimization (ESO) in 1992, to solve optimization problems by gradually removing elements with lowest value of von-Mises stress until the desired volume fraction is reached [45]. In 1996, stiffness-constrained optimization problems were solved using ESO, where the sensitivity number of each element was calculated using strain energy [46].

Querin et al. expanded the "hard-killing" ESO to BESO, which allowed the discarded elements to be re-added under certain circumstances [47]. An AESO approach was introduced in [48] which instead of discarding elements from a larger-than-optimum design, added elements to a minimum base design. In AESO, unlike ESO one could use maximum criterion directly in evolution process. Liu et al. developed a GESO algorithm, wherein a chromosome array was assigned to each element, and an element was removed only if all values of genes were zero [49]. The salient features of the ESO family are that they do not introduce intermediate elements and do not compute gradients. Thus, most of these methods fall into the category of non-gradient topology optimization (NGTO) methods, whose deficiencies are addressed in [50].

Element Sensitivity Methods for MMTO. In 2010, Ramani developed an algorithm for compliance minimization for multiple materials [51]. The algorithm starts with computing and ranking element sensitivities, where for each element, there are generally two values defined as sensitivity to change from current state to an immediate step, both better and worse performance. Then material distribution undergoes a repeated cycle between feasible and infeasible solutions until it converges. Ramani extended his work in 2011 to stress-constrained multi-material topology optimization [52].

The present work once again uses the concept of element sensitivity, as in [51]. However:

1. The connection between element sensitivity and well-known topological sensitivity is illustrated in this paper. Further, the element sensitivity is generalized to arbitrary quantities of interest.
2. In [51], the intermediate designs may be structurally disconnected. Therefore, as the author states, it is critical that void elements be assigned a low value of Young's modulus. In the present work, by construction, every intermediate design is connected, and void elements can be suppressed without resulting in singularity. This leads to better condition number, and faster convergence.
3. Displacement constraint are handled in [51] by switching between 'infeasible' and 'feasible' designs. In this paper, all intermediate designs satisfy the displacement constraint. Thus, the designer has the option of choosing from a multitude of Pareto-optimal designs, as the numerical experiment later illustrates.
4. The material changes in [51] are restricted; this may lead to sub-optimal designs; this is illustrated later through numerical experiments.

3. PROPOSED STRATEGY

In this paper we generalize the single-material Pareto tracing method of topology optimization proposed in [15], [16] to multiple materials.

3.1 Pareto Method for SMTO

Consider the following single-material topology optimization problem, where the goal is to find the best possible topology with respect to compliance (J) and volume (or weight):

$$\begin{aligned} &\underset{\Omega \subset D}{Min}\{J, |\Omega|\} \\ &\text{subject to} \\ &Ku = f \\ &J = f^T u \end{aligned} \tag{4}$$

Using the concept of topological sensitivity [53], a topological level set method was developed in [15], [16] for SMTO that traces the Pareto curve governing compliance and volume fractions. The Pareto-optimal designs do not exhibit 'islands', which results in better conditioned stiffness matrices, and consequently faster iterative convergence. Figure 3 illustrates the Pareto curve, and computed topologies, for the problem in Figure 2. The properties of material A is given in Table 1. Given the computational advantages and robustness of this method for single material optimization (see[16], [54], [55] for supportive evidence), the objective of this paper is to generalize this to multiple materials.

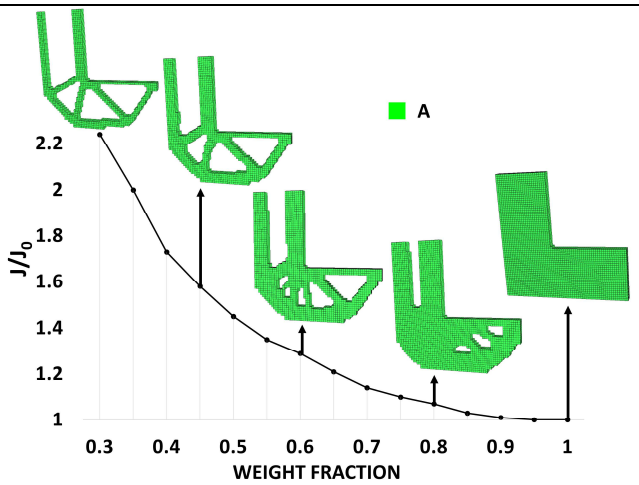

Figure 3: The Pareto-optimal curve and topologies for a single material (A).

3.2 Topological vs. Element Sensitivities

Towards this end, one can consider generalizing the concept of topological sensitivity to both anisotropic and multiple materials. Anisotropic material was first addressed in [56], and composite material was addressed in [57]. However, computing closed-form expressions for topological sensitivity for arbitrary material distribution is non-trivial. We therefore consider an alternate and well known concept of "element sensitivity" that is easy to

compute for arbitrary material distributions, and easy to generalize to arbitrary quantities of interest.

Specifically, consider the 2D equivalent of the L-Bracket problem posed in Figure 2. The topological sensitivity is defined as the first order change in compliance when an infinitesimal hole is inserted, leading to the expression [15]:

$$\mathcal{T}^S(p) = \frac{4}{1+\nu}\sigma : \varepsilon - \frac{1-3\nu}{1-\nu^2} tr(\sigma) tr(\varepsilon) \tag{5}$$

This field is illustrated in Figure 4a, where the stresses and strains are computed at the center of each element.

On the other hand, the element sensitivity is the expected change in compliance when an element is deleted from the mesh. This, one can show is given by (see [3]):

$$\Delta J = u_e^T K_e u_e \tag{6}$$

where u_e is the element displacement and K_e is the element stiffness matrix. The element sensitivity field is illustrated in Figure 4b. Observe the similarities between the two fields in Figure 4; the scaling is not important since the optimization process is scale independent. Thus the element sensitivity field can also be treated as a level set.

The similarity between the two fields is not surprising since they fundamentally capture the expected change in a compliance when material is deleted. There are, of course, several differences between the two. Perhaps, the most important one is that the element sensitivity is easy to generalize to arbitrary materials, and quantities of interest (see Appendix A), while the former is a lot harder.

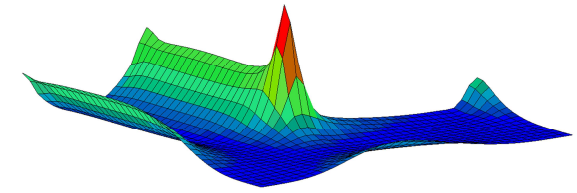

(a) Plot of 2D topological sensitivity field.

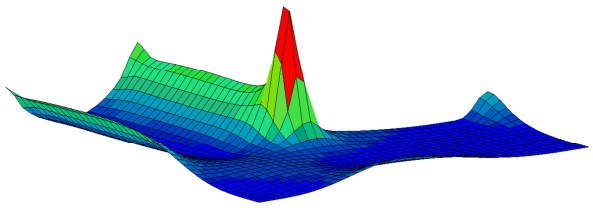

(b) Plot of 2D element sensitivity field.

Figure 4: Topological and element sensitivity fields for the single-material 2D L-Bracket problem.

For multiple materials, the element sensitivity is generalized in Section 3.4 as the expected change in a quantity of interest when the underlying material is changed (rather than deleted). Formally, this can be interpreted as a multi-colored level-set [38], and can be used as a basis for continuous optimization.

However, for computational efficiency, we propose and justify a simple approximation for exploiting the multi-colored element-sensitivities. Several experiments illustrate the effectiveness of this approximation.

3.3 Formulation

The classic approach to MMTO is to minimize compliance subject to two sets of constraints: (1) a total volume constraint, and (2) individual volume fraction constraint on each of the material constituents. The latter can artificially restrict the design space. More recently, researchers have explored mass constraint formulations [51], [58].

Here, we consider any pair of conflicting objectives (for example, mass and compliance), and the corresponding Pareto curve is traced. No additional constraint is imposed on the material composition, providing additional freedom during optimization.

The first objective is generically referred to as *cost* (C); this includes quantities such as total mass or total price. The second objective is referred to as *inefficiency* (I), i.e., the inverse of performance; this captures quantities such as compliance, p-norm stress, etc. The goal is to minimize both cost and inefficiency. In other words, a two-objective multi-material problem is posed as:

$$\begin{aligned} &\underset{\Omega_{k=1,2..M} \subset D}{Min} \{I, C\} \\ &\Omega_i \cap \Omega_{j \neq i} = \varnothing \\ &\text{subject to} \\ &Ku = f \end{aligned} \tag{7}$$

For example, the compliance (J) versus weight (W) problem is:

$$\begin{aligned} &\underset{\Omega_{k=1,2..M} \subset D}{Min} \{J, W\} \\ &\Omega_i \cap \Omega_{j \neq i} = \varnothing \\ &\text{subject to} \\ &Ku = f \\ &J = f^T u \end{aligned} \tag{8}$$

Our objective will be to trace the Pareto curve involving these two quantities with cost (C) on the x axis and inefficiency (I) on the y axis. The proposed algorithm will start with a topology with the highest cost; then: (1) the cost function will be reduced by a small decrement (sub-algorithm 1), followed by (2) a reduction in inefficiency while keeping cost a constant (sub-algorithm 2); these two steps are illustrated in Figure 5. By repeating these two steps, the Pareto curve is traced and numerous topologies that lie on the curve are computed in an efficient manner.

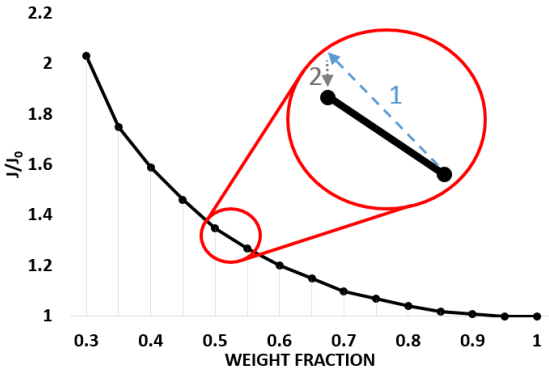

Figure 5: Tracing the Pareto curve, and the two sub-steps.

3.4 Terminology

In this section, we introduce the necessary terminology before describing the algorithm in detail. We assume the underlying

design has been discretized using finite elements, and each element can be associated with a material of choice.

We will now establish the concept behind the two steps illustrated in Figure 5. Suppose we have a finite element with material *k* within the design. We will now consider a hypothetical swapping of the underlying material *k* to material *m*. Observe that the change in compliance (*I* is used here to denote inefficiency) is given by the first-order element sensitivity (see Appendix A):

$$\triangle I_e^{k\to m} = u_e^T K_e^k u_e - u_e^T K_e^m u_e \tag{9}$$

As a special case, if the element is deleted, i.e., replaced with void, we have:

$$\triangle I_e^{k\to \varnothing} = u_e^T K_e^k u_e \tag{10}$$

Similarly, as a special case of Equation (9), if a new element is inserted (in place of a void):

$$\triangle I_e^{\varnothing\to m} = -u_e^T K_e^m u_e \tag{11}$$

Note that the above equation is consistent with the sensitivity expressions used in SIMP for compliance [3]; also see [59].

The element sensitivity in Equation (9) can obviously be generalized to other quantities of interest. Specifically, for any quantity of interest *Q*, the first-order sensitivity is given by (see Appendix A):

$$\triangle Q_e^{k\to m} = -\lambda_e^T K_e^k u_e + \lambda_e^T K_e^m u_e \tag{12}$$

where λ is the adjoint field [60] associated with the quantity of interest. Thus, there is no fundamental restriction of the proposed method to compliance problems. The specific expression for the adjoint depends on the quantity of interest; for example, for the p-norm stress, an expression for the adjoint is derived in [54].

Correspondingly, the change in cost can also be computed; for example, if the cost is the weight function:

$$\triangle C_e^{k\to m} = \rho^m V_e - \rho^k V_e \tag{13}$$

where ρ denotes (real) material density and V_e denotes volume of an element.

Now consider the cost-inefficiency plot of Figure 6. Recall that we start with a topology and material choice with the highest cost; therefore our objective is to constantly reduce cost, i.e., we swap materials only if $\Delta C_e^{k\to m} < 0$.

The change in inefficiency can be either positive or negative. Therefore, only quadrants 2 and 3 in Figure 6 are acceptable; quadrant 3 is preferrable, since both cost and inefficiency are reduced. Thus the angle θ must be maximized, i.e.,

$$\begin{aligned} &\underset{m}{Max}\ \theta_e^{k\to m} \equiv \frac{\Delta I_e^{k\to m}}{\Delta C_e^{k\to m}} \\ &\text{subject to} \\ &\Delta C_e^{k\to m} < 0 \end{aligned} \tag{14}$$

or equivalently:

$$\begin{aligned} &\underset{m}{Min}\ -\theta_e^{k\to m} \equiv \frac{-\Delta I_e^{k\to m}}{\Delta C_e^{k\to m}} \\ &\text{subject to} \\ &\Delta C_e^{k\to m} < 0 \end{aligned} \tag{15}$$

Hence, in the first sub-step, for each element, we find the material *m* that gives the lowest value of $-\theta_e^{k\to m}$.

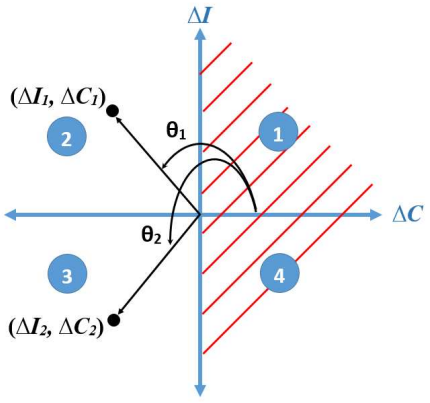

Figure 6: Feasible regions w.r.t change in inefficiency and cost.

In the second sub-step, we reduce inefficiency while keeping cost a constant. To do so, we find elements that are outside the current design, but adjacent to the boundary. Next, for each such element (e^{out}), we find an inside element (e^{in}) with the same material, that gives the lowest value of change in inefficiency:

$$\Delta I_{e^{in}\rightleftarrows e^{out}}^{k\to k} = u_{e^{in}}^T K_{e^{in}}^k u_{e^{in}} - u_{e^{out}}^T K_{e^{out}}^k u_{e^{out}} \tag{16}$$

For the second sub-algorithm note that:

- For e^{out} we can either extrapolate or use the last updated properties of the element. Here, we have used the last updated material and field solution prior to deletion.
- For a voxelized mesh, in order to keep cost a constant, it is suficient that both elements have the same material *k*.

3.5 Optimization Algorithm

The main algorithm is illustrated in Figure 7 and each of the steps is described below.

0. Start with an initial design with $\Omega = D$ and maximum cost (example, maximum weight).
1. The cost C is reduced by ΔC, either by removing material or replacing the most costlier material one with the less expensive one (see sub-step 1 for details).
2. While keeping C constant, some of the deleted elements are brought back if it reduces (see sub-step 2 for details)
3. Check if the converged design is acceptable:
4. If Step-3 fails, reduce ΔC and repeat
5. If the design has converged to the desired cost C, optimization is terminated
6. (Else) ΔC is reinitialized, and algorithm returns to step-1.

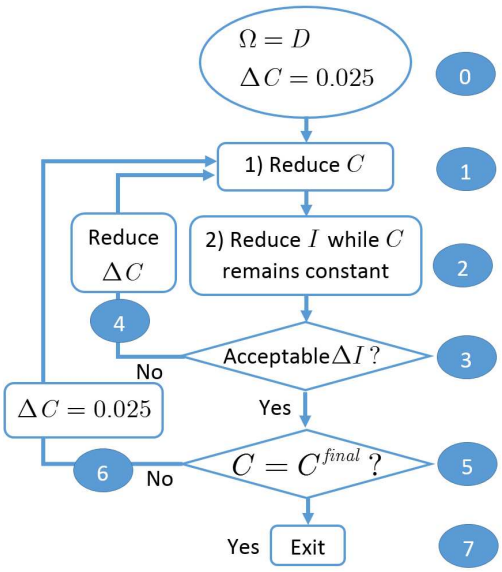

Figure 7: Main algorithm

Sub-step 1: Reduce Cost C. The sub-algorithm 1 is illustrated in Figure 8, and each of the steps is described below.

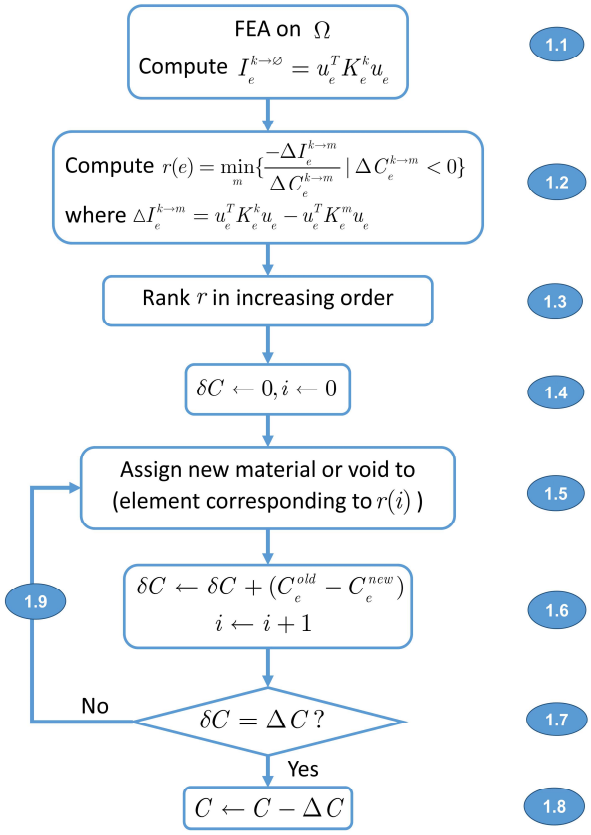

Figure 8: Sub-algorithm 1, reducing C.

1.1 We first perform a finite element analysis and compute the inefficiency for each element' for compliance, we have

$$I_e^{k\to\varnothing} = u_e^T K_e^k u_e$$

1.2 Next, for each element we find the ranking parameter such that:

$$r(e) = \min_m\{\frac{-\Delta I_e^{k\to m}}{\Delta C_e^{k\to m}} \mid \Delta C_e^{k\to m} < 0\}$$

In other words, $r(e)$ gives the best possible choice of material change for element e .

1.3 In the next step, we sort the array r in an increasing order while keeping track of corresponding material and element.

1.4 Initialize counter *i* and the current reduction in C in this step (δC) to zero.

1.5 Replace elements with a new material or void, accordingly.

1.6 Update values of δC and *i*.

1.7 Check if we have reached the allowed ΔC .

1.8 (Yes) Update C and go to sub-step 2

1.9 (No) return to 1.5

Sub-step 2: Reduce Inefficiency at Constant C. Figure 9 shows the sub-algorithm 2, and each of its steps is explained herein.

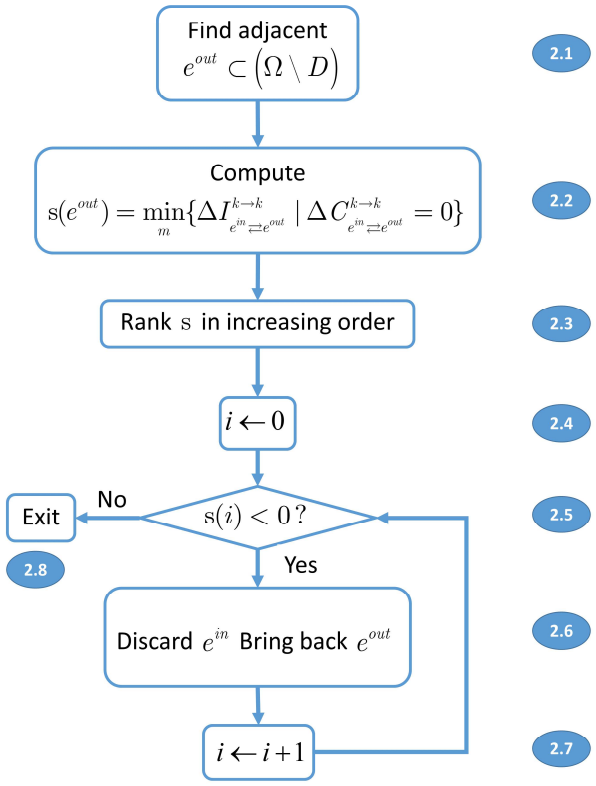

Figure 9: Sub-algorithm 2, increasing Performance while keeping C constant .

2.1 Find the elements which are the potential candidates to be brought back, that is, find the elements that are already discarded in the optimization process but are immediate neighbors to the current domain.

2.2 For each candidate (e^{out}), find the ranking parameter s such that:

$$\mathrm{s}(e) = \min_{m}\{\Delta I^{k\to k}_{e^{in}\rightleftarrows e^{out}} \mid \Delta C^{k\to k}_{e^{in}\rightleftarrows e^{out}} = 0\}$$

where 'k' is the last material e^{out} had before it was discarded.

2.3 Sort s in increasing order.

2.4 Initialize index i

2.5 Check if the i^{th} entry of s is negative:

2.6 (Yes) Discard e^{in} and re-add e^{out} .

2.7 (Yes) Move to next entry in s and return to 2.3

2.8 (No) Exit sub-step

The complexity of Step 2.2 is O(m*n) where 'm is the number of elements that lie outside the current design/topology, but are adjacent to the boundary, while 'n' is the number of elements that lie inside the current design/topology.

3.6 Matrix-Free FEA, Voxelization, and Deflated CG

In this Section, we briefly describe a few implementation details. In classic finite element analysis (FEA), the element stiffness matrices are typically assembled into global stiffness matrix K . In the present paper, we will apply matrix-free (or assembly-free) FEA, where K is neither assembled nor stored. Instead, the fundamental matrix operations such as the sparse matrix-vector multiplications (SpMV) are carried out in an elemental level. For instance, SpMVs are typically implemented by first assembling the element stiffness matrices as follows:

$$Kx = \left(\sum_{e} K_e\right)x \tag{17}$$

In an assembly free method, this is implemented by first carrying out the multiplications at the elemental level, and then assembling the results:

$$Kx = \sum_{e}(K_e x_e) \tag{18}$$

In other words, instead of assembling the global matrix, and then performing SpMV, an element-vector multiplication is carried, and then the results are assembled. This idea was first proposed in 1983 [61], but has been resurfaced due to the advent of multi-core architectures. Further, we consider a simple finite element discretization, where the geometry is approximated via uniform hexahedral elements or 'voxels'; the voxel-approach has gained significant popularity recently due to its robustness and low memory foot-print. The more significant benefits of voxelization are: (1) it is robust in that the automatic mesh generation rarely fails (unlike traditional meshing), (2) the mesh storage is compact, (3) the cost of voxelization is usually negligible and is relatively insensitive to geometric complexity, (4) it promotes assembly-free-FEA [62], [63], and (5) it simplifies the proposed optimization algorithm.

Moreover, we use conjugate gradient (CG) method to solve the FEA linear system of equations. For acceleration, we rely on deflation [64]. Deflation is a powerful acceleration technique for CG, and is more suitable for the assembly-free FEA than classic preconditioners such as incomplete Cholesky. In this paper, we use a deflation method based on rigid-body deflation presented in [62].

3.7 Filtering

To overcome the ill-posedness in topology optimization, different filtering techniques have been proposed [3]. In the present work, two filtering schemes are employed:

a) **Sensitivity filtering**: Once the element sensitivities are computed for each element, the node sensitivity is computed by averaging the neighboring element sensitivities. The element sensitivities are then re-computed by averaging the node sensitivities. This is repeated N times, where N is determined by the filter radius 'r' and the mesh element size h:

$$N = \max\left(1, \frac{r}{h}\right) \tag{19}$$

In this paper, the filter radius was chosen to be 3*h, resulting in a typical value of 3 for N.

b) **Morphological filtering**: Once the final topology is computed, we use morphological filtering to enhance the manufacturability of the design. This idea was used by Sigmund [65] to prevent the grey transition regions in SIMP. While Sigmund [65] discussed the 2D filtering, the extension to 3D is straightforward; in this paper, we use the 17-element "structuring element" illustrated in Figure 10.

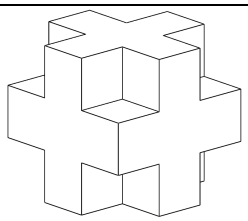

Figure 10: 3D structuring element for morphological filtering.

4. NUMERICAL EXPERIMENTS

In this section, we demonstrate the validity of the proposed method through several 3D examples.

In Section 4.1, the single-material compliance minimization of the classic L-bracket is compared against a two-material compliance minimization. This experiment illustrates that, for a given weight fraction, the two-material design is less compliant (i.e., stiffer) than the single material design. In addition, the condition numbers of the underlying stiffness matrices for single and multiple materials are compared.

In Section 4.2, the effectiveness of the filtering method is illustrated through a mesh independency study on the classic MBB structure.

In Section 4.3, three materials are considered for a benchmark problem. As expected, for a given weight-fraction, adding a material choice improves the performance.

In Section 4.4, we consider the three-material C-Bracket problem posed in [51] where an additional displacement constraint is imposed. We show that the proposed method yields a lower weight design, and discuss the underlying reasons.

In Section 4.5, orthotropic materials are considered and illustrated. Once again, the advantage of using multiple materials is emphasized.

Finally, in Section 4.6, the computational costs (running time and memory required) for all the above experiments are summarized.

In all numerical experiments, the decrement in the cost function for Pareto tracing is initialized to 0.025. All dimension are in meters, unless otherwise noted. In all tables, E , ν , and ρ denote Young's modulus, Poisson ratio, and density, respectively. For all experiments, we rely on the assembly-free deflated conjugate gradient (CG) discussed in [62], with a tolerance set to 10^{-8}.

4.1 L-Bracket: Single and Two-Material Design

First, we consider the L-bracket illustrated in Figure 2. The Pareto curve is generated using: (1) a single material A, and (2) two materials A and B, whose properties are summarized in Table 1. The weight serves as the cost function while compliance is minimized; 20,000 elements are used for both experiments.

Table 1: Material Properties of A and B.

Material	$E\ (GPa)$	υ	$\rho\ (\mathrm{Kg/m^3})$
A	170	0.3	7100
B	70	0.33	2700

As stated earlier in the algorithm, we start with the heaviest design (all A) and optimize the topology and material distribution. After the optimization process is complete, we obtain the two Pareto curves illustrated in Figure 11. As expected, for a given weight fraction, the two-material design is less compliant (stiffer) than the corresponding single material design.

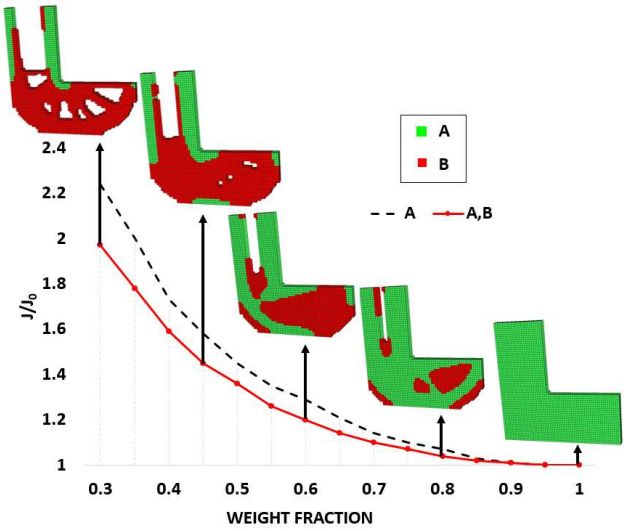

Figure 11: The Pareto curves and topologies for single material (A) and two materials (A and B).

For the above two experiments, Figure 12 illustrates the number of deflated CG iterations for each of the 32 FEAs during optimization. Figure 12a corresponds to single-material, while Figure 12b corresponds to multi-material. As one can observe, the iterations increase moderately in both scenarios; this can be attributed to the presence of thin/slender structures in the topology. Both experiments required 32 finite element operations to complete. Thus, for this example, the cost of multi-material design is almost exactly the same as the single-material design.

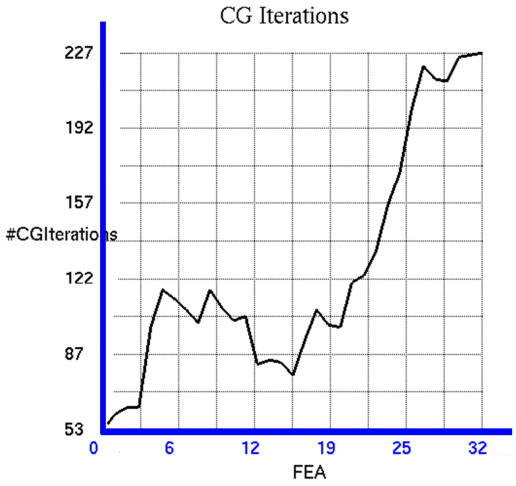

(a) CG iterations for single-material design.

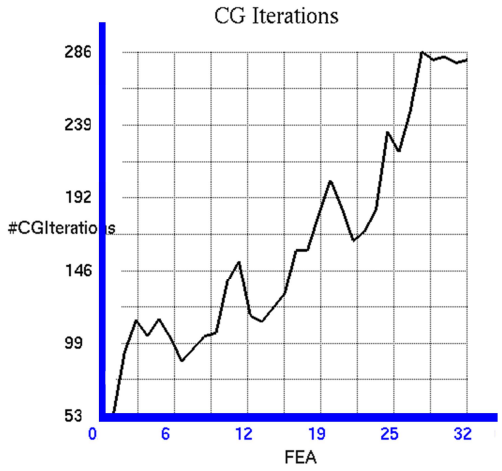

(b) CG iterations for two-material design.

Figure 12: CG iterations for the L-Bracket with (a) single material A, (b) two materials A and B.

4.2 MBB Structure: Mesh Independency

In this example, we study the impact of mesh size using the classic MBB structure illustrated in Figure 13. The structure is loaded with 30 units at the center, and 15 units on either side of the center; the material properties are given in Table 1.

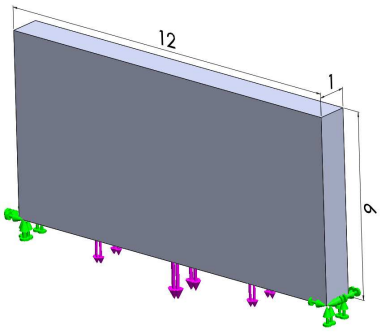

Figure 13: MBB structure.

Figure 14 illustrates the Pareto curves with 10,000 and 40,000 elements; as one can observe, the two curves are almost identical, suggesting that the method is insensitive to mesh discretization.

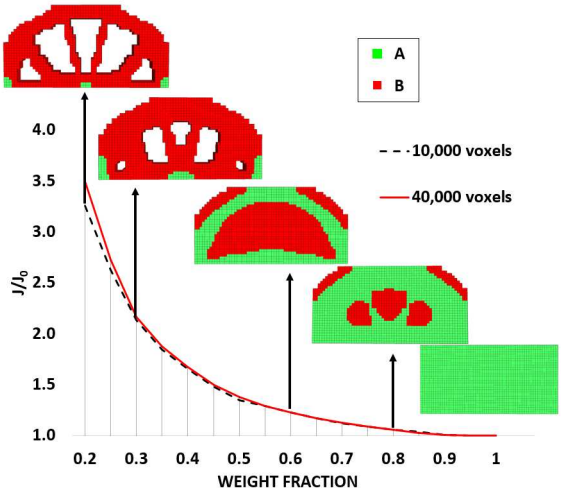

Figure 14: Pareto curves for 10,000 and 40,000 elements.

The final topologies are illustrated in Figure 15. Note that as the mesh size increases, the design details are a bit refined as expected. Yet the distribution of the material within the two designs are quite similar.

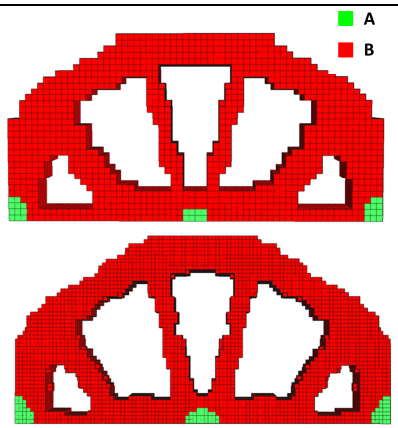

Figure 15: MBB structure with 10,000 and 40,000 elements at weight fraction of 0.2.

4.3 Cantilevered Beam: Three-Material Pareto Curve

In this experiment, we consider three materials. The geometry and boundary conditions are illustrated in Figure 16. The design is discretized using 10,000 elements, i.e. 34020 degrees of freedom (dof).

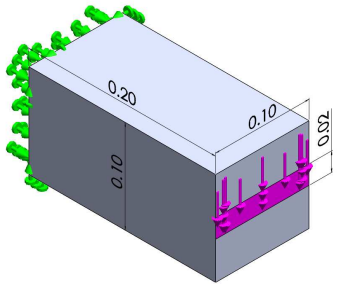

Figure 16: Cantilevered beam.

The material properties are summarized in Table 2. We solve the MMTO problem for 3 different scenarios: (1) pure A (single material), (2) A and B (two materials) and (3) A, B, and C (three materials).

Table 2: Material Properties of A, B and C

Material	$E\ (GPa)$	υ	$\rho\ (\mathrm{Kg/m^3})$
A	380	0.2	19250
B	210	0.3	7800
C	110	0.25	4390

Figure 17 illustrates the three Pareto curves, and the topologies for the third scenario. As one can observe, moving from one material to two-materials results in a significant improvement, while adding the third-material results in a slight improvement.

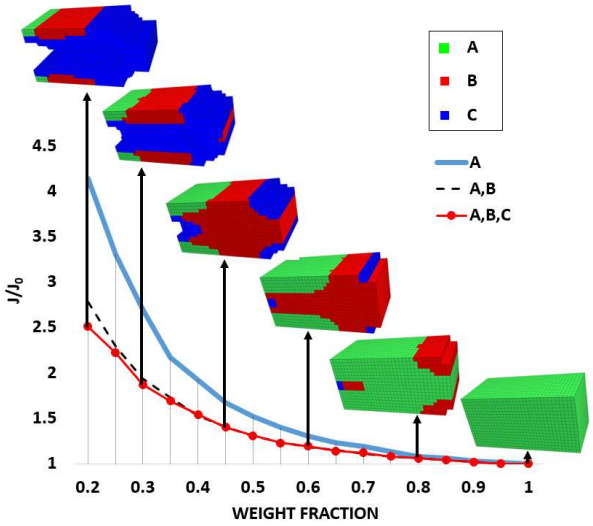

Figure 17: Effect of number of materials on Pareto Curve

4.4 C-Bracket: Displacement Constraint

In this experiment, we consider the C-bracket problem posed in [51]. The geometry and boundary conditions are illustrated in Figure 18 (units in meters), with a load of 10 N, while Table 3 summarizes the material properties. The initial all-steel design weighs about 27.7 grams, with a maximum deflection of about $8.3*10^{-7}$ m. The objective is to find the lightest combination of materials and topology such that the deflection does not exceed 10^{-5} m. Observe that there are no restriction on volume fractions of materials used.

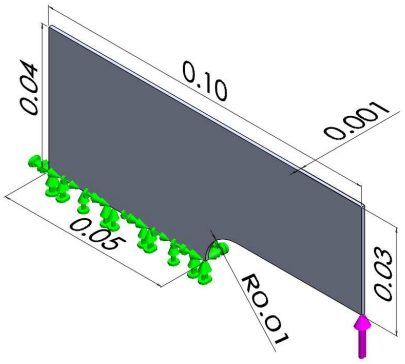

Figure 18: C-Bracket problem considered in [51].

Table 3: Material Properties of Steel, Aluminum, Magnesium

Material	$E\ (GPa)$	υ	$\rho\ (\mathrm{Kg/m^3})$
Steel	210	0.3	7890
Aluminum	70	0.3	2630
Magnesium	44	0.3	1740

In [51], the equivalent 2D plane-stress problem was considered with about 3300 quadrilateral elements. Here, we consider the problem in 3D since our implementation is limited to 3D. Due to the high aspect ratio, a total of 8,000 3D linear hexahedral elements was used here to discretize the domain.

Figure 19 illustrates the convergence of the C-Bracket. The final design weighs 4.4 gm using a combination of steel and aluminum. This can be compared against the result of 4.7 gm obtained in [51]. In both cases, the displacement constraints are satisfied.

The design computed here uses only Steel and Aluminum (although Magnesium is offered as a 3rd material of choice). However, in [51] all three materials are deployed in the final design. This may be attributed perhaps to the fact that material changes in [51] are more restrictive.

A second difference between the proposed method and the method described in [51] is that in [51], many of the intermediate designs are infeasible, i.e., they violate the displacement constraint. However, in the proposed method, all intermediate designs satisfy the constraint. Thus, the designer has the option of choosing from a multitude of Pareto-optimal designs with varying performance.

The number of iterations of the two methods are comparable: 50 iterations in [51], compared to 41 iterations in the proposed method.

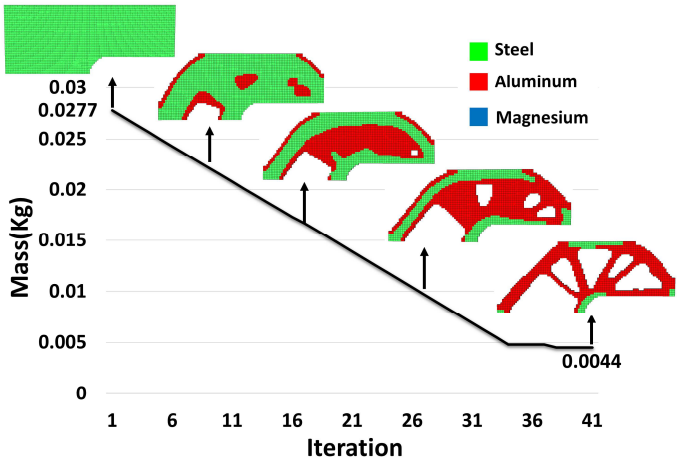

Figure 19: Convergence plot of C-Bracket

4.5 Table Design: Orthotropic Materials

We now consider the use of orthotropic materials. Specifically, consider the table design problem posed in Figure 20, where a uniform vertical pressure is applied on the top-face, and the four bottom corners are restrained. The domain is discretized into 20,000 elements. In practice, for such problems, one must also consider self-weight during optimization, but this is neglected in this paper.

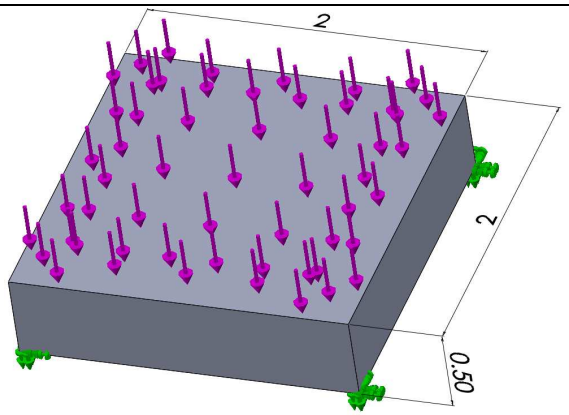

Figure 20: Table design geometry and boundary conditions

In this experiment, we use price as the cost metric, and stiffness as the performance metric. Mechanical properties of A and C are given in Table 4, while the properties of B (an orthotropic material with unidirectional fibers) are summarized in Table 5. Since are using price as the cost metric rather than weight, the densities are not relevant. The relative prices for the three materials are given in Table 6.

Table 4: Mechanical properties of steel and plastic

Material	$E\ (GPa)$	υ
A	210	0.3
C	10	0.45

Table 5: Mechanical properties of B

Parameter	Value
$E_{11}, E_{12} (GPa)$	130, 20
$G_{12}, G_{22}\ (GPa)$	6, 9.5
$\upsilon_{12}, \upsilon_{23}$	0.01,0.05

Table 6: Price list

Material	Relative Price
A	100
B	75
C	25

To generate the Pareto-curve, we start with the design with the largest cost; in this case, with an all-A design space. The objective is to find both a single-material (A) design and three-material design (A, B, and C) with a price target of 24% of initial cost. When a single-material (A) is used, Figure 21 illustrates the final design, with the target price.

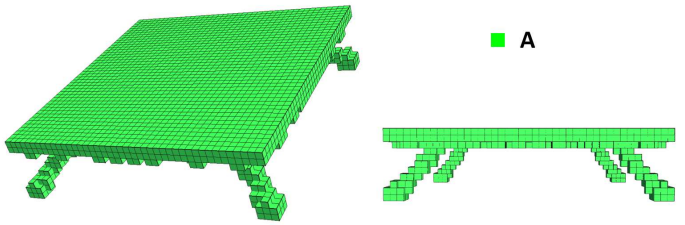

Figure 21: Table design using a single material

Figure 22 illustrates the final design using three materials. *Both designs cost exactly the same, but the design with multi-materials in Figure 22 is 3.0 times stiffer than that of a single-material in Figure 21.*

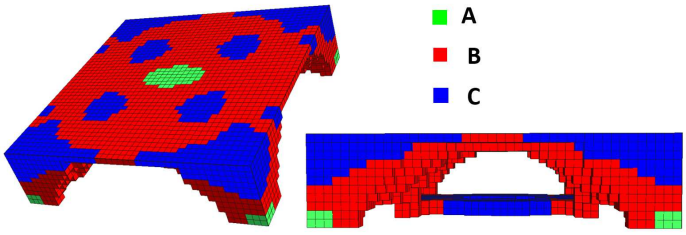

Figure 22: Table design using three materials.

4.6 Run times and Memory Requirements

For all the experiments presented in this section, Table 7 summarizes the degrees of freedom, the target weight (or cost), total run-time, and required memory. All experiments were conducted on an Intel Core i7 CPU running at 3.4 GHz with 8GB of memory. Observe that all of the optimizations are completed in about a minute, and use the limited memory (in the order of a tens of Mega-Bytes).

Table 7: Summary of computational costs.

Expt.	*#DOF*	*Target Wt./Cost*	*Time (secs)*	*Memory (MB)*
L-Bracket	41,730	30%	24	40
MBB	36,288	20%	79	30
Beam	34,020	20%	33	30
C-Bracket	32,976	14%	58	10
Table	69,696	24%	83	60

5. SUMMARY AND FUTURE WORK

The method discussed in this paper traces the multi-material Pareto curve involving two conflicting objectives such as stiffness and weight (or stiffness and price). The element sensitivity is used to drive the optimization process. While the element sensitivity field can be treated as a multi-colored level set, for computational efficiency, we propose and justify a simple heuristic for discrete element-swapping. The effectiveness and robustness of this method is demonstrated via a number of 3D examples, involving isotropic and orthotropic materials.

The proposed algorithm generates topologies defined by a set of voxels with distinct material properties. This is in contrast to classic boundary representation typically used for capturing topologies with isotropic material. Further, the voxel based topologies generated here can directly be processed by voxel-based g-code generators, for example, the OpenFab pipeline [13], and this is being explored.

Future work will also focus on other performance metrics, considering multiple load cases and multiple constraints. Further, before this method can be deployed in AM, potential de-bonding, stress residuals, feature size, and other AM-related issues must be accounted for.

Appendix A: Element Sensitivity

The derivation of Equation (12) is included here for completeness. Consider the problem:

$$Ku_0 = f \tag{20}$$

Suppose an element is deleted from the mesh, this will lead to a change in K, resulting in:

$$(K - \Delta K_e)(u_0 + \Delta u) = f \tag{21}$$

Formally:

$$(u_0 + \Delta u) = (K - \Delta K_e)^{-1} f \tag{22}$$

As a formal Neumann series:

$$(u_0 + \Delta u) = \left[u_0 + \left(K^{-1}\Delta K_e\right)u_0 + \left(K^{-1}\Delta K_e\right)^2 u_0 + \ldots\right] \tag{23}$$

Neglecting higher order terms

$$\Delta u \approx \left(K^{-1}\Delta K_e\right)u_0 \tag{24}$$

Now consider a quantity of interest:

$$Q(u) \tag{25}$$

The first order change in the quantity of interest is defined via its gradient with respect to the displacement:

$$\Delta Q \approx \left(\nabla_u Q\right)^T \Delta u \tag{26}$$

Substituting Equation (24) into above, and taking the transpose:

$$\Delta Q \approx \left(K^{-1}\nabla_u Q\right)^T \left(\Delta K_e\right)u_0 \tag{27}$$

Defining the adjoint as:

$$\lambda_0 = -K^{-1}\nabla_d Q \tag{28}$$

We have:

$$\Delta Q \approx -\lambda_0^T \Delta K_e u_0 \tag{29}$$

The above equation captures the first order change in any quantity of interest when an element is deleted. When an element is inserted, the sign changes:

$$\Delta Q \approx \lambda_0^T \Delta K_e d_0 \tag{30}$$

From Equations (29) and (30) follows Equation (12) for element swapping (deleted one material and add the other). As a special case when the quantity of interest is the compliance, we have:

$$Q(u) = f^T u \tag{31}$$

Therefore:

$$\nabla_u Q = f \tag{32}$$

And the adjoint is given by:

$$\lambda_0 = -K^{-1} f = -u \tag{33}$$

By substituting Equation (33) in Equation (12), we obtain Equation (9).

ACKNOWLEDGEMENT

The authors would like to thank the support of National Science Foundation through grants CMMI-1232508 and CMMI-1161474.

REFERENCES

[1] H. A. Eschenauer and N. Olhoff, "Topology optimization of continuum structures: A review," *Applied Mechanics Review*, vol. 54, no. 4, pp. 331–389, 2001.

[2] G. I. N. Rozvany, "A critical review of established methods of structural topology optimization," *Structural and Multidisciplinary Optimization*, vol. 37, no. 3, pp. 217–237, 2009.

[3] M. Bendsøe and O. Sigmund, *Topology Optimization: Theory, Methods and Application*, 2nd ed. Springer, 2003.

[4] E. Kesseler, "Multidisciplinary design analysis and multi-objective optimisation applied to aircraft wing," *WSEAS transactions on systems and Control and Cybernetics*, vol. 1, no. 2, p. 221 227, 2006.

[5] J. J. Alonso, "Aircraft design optimization," *Mathematics and Computers in Simulation*, vol. 79, no. 6, pp. 1948–1958, 2009.

[6] V. H. Coverstone-Carroll, "Optimal multi-objective low-thrust spacecraft trajectories," *Comput. Methods Appl. Mech. Eng.*, vol. 186, pp. 387–402, 2000.

[7] L. Wang, "Automobile body reinforcement by finite element optimization," *Finite Elements in Analysis and Design*, vol. 40, no. 8, pp. 879 – 893, 2004.

[8] G. K. Ananthasuresh, S. Kota, and Y. Gianchandani, "A methodical approach to the design of compliant micromechanisms," in *Solid State Sensor and Actuator Workshop*, 1994, pp. 189–192.

[9] S. Nishiwaki, "Topology Optimization of Compliant Mechanisms using the Homogenization Method," *International Journal for Numerical Methods in Engineering*, vol. 42, pp. 535–559, 1998.

[10] T. E. Bruns and D. A. Tortorelli, "Topology optimization of non-linear elastic structures and compliant mechanisms," *Computer Methods in Applied Mechanics and Engineering*, vol. 190, no. 26–27, pp. 3443–3459, 2001.

[11] Z. Luo, "Compliant mechanism design using multi-objective topology optimization scheme of continuum structures," *Structural and Multidisciplinary Optimization*, vol. 30, pp. 142–154, 2005.

[12] I. Gibson, D. W. Rosen, and B. Stucker, *Additive Manufacturing Technologies*. Springer, 2010.

[13] K. Vidimce, S.-P. Wang, J. Ragan-Kelley, and W. Matusik, "OpenFab: A Programmable Pipeline for Multi-Material Fabrication," *SIGGRAPH/ACM Transactions on Graphics*, vol. 32, no. 4, 2013.

[14] J. Thomsen, "Topology optimization of structures composed of one or two materials," *Journal of Structural Optimization*, vol. 5, pp. 108–115, 1992.

[15] K. Suresh, "A 199-line Matlab code for Pareto-optimal tracing in topology optimization," *Structural and Multidisciplinary Optimization*, vol. 42, no. 5, pp. 665–679, 2010.

[16] K. Suresh, "Efficient Generation of Large-Scale Pareto-Optimal Topologies," *Structural and Multidisciplinary Optimization*, vol. 47, no. 1, pp. 49–61, 2013.

[17] M. P. Bendsøe and N. Kikuchi, "Generating optimal topologies in structural design using a homogenization method," *Computer Methods in Applied Mechanics and Engineering*, vol. 71, pp. 197–224, 1988.

[18] O. Sigmund, "A 99 line topology optimization code written in Matlab," *Structural and Multidisciplinary Optimization*, vol. 21, no. 2, pp. 120–127, 2001.

[19] G. Allaire, F. Jouve, and A. M. Toader, "A level-set method for shape optimization," *Comptes Rendus Mathematique*, vol. 334, no. 12, pp. 1125–1130, 2002.

[20] G. Allaire and F. Jouve, "A level-set method for vibration and multiple loads structural optimization," *Structural and Design Optimization*, vol. 194, no. 30–33, pp. 3269–3290, 2005.

[21] L. He, C.-Y. Kao, and S. Osher, "Incorporating topological derivatives into shape derivatives based level set methods," *Journal of Computational Physics*, vol. 225, no. 1, pp. 891–909, 2007.

[22] M. Y. Wang, X. Wang, and D. Guo, "A level set method for structural topology optimization," *Computer Methods in Applied Mechanics and Engineering*, vol. 192, pp. 227–246, 2003.

[23] H. Hamda, "Application of a multi-objective evolutionary algorithm to topology optimum design," in *Fifth International Conference on Adaptive Computing in Design and Manufacture*, 2002.

[24] Y. M. Xie, "A simple evolutionary procedure for structural optimization," *Computers and Structures*, vol. 49, no. 5, pp. 885–896, 1993.

[25] Y. M. Xie and G. P. Steven, *Evolutionary Structural Optimization*, 1st ed. Berlin: Springer-Verlag, 1997.

[26] N. P. van Dijk, K. Maute, M. Langelaar, and F. van Keulen, "Level-set methods for structural topology optimization: a review," *Structural and Multidisciplinary Optimization*, vol. 48, no. 3, pp. 437–472, 2013.

[27] O. Sigmund and K. Maute, "Topology Optimization Approaches," *Structural and Multidisciplinary Optimization*, vol. 48, no. 6, pp. 1031–1055, 2013.

[28] J. K. Guest, "Achieving minimum length scale in topology optimization using nodal design variables and projection functions," *International Journal of Numerical Methods in Engineering*, vol. 61, no. 2, pp. 238–254, 2004.

[29] T. Nguyen, G. Paulino, J. Song, and C. Le, "A computational paradigm for multiresolution topology optimization (MTOP)," in *Structural and Multidisciplinary Optimization*, vol. 41, 2010, pp. 525–539.

[30] F. V. Stump, E. C. N. Silva, and G. Paulino, "Optimization of material distribution in functionally graded structures with stress constraints," *Communications in Numerical Methods in Engineering*, vol. 23, no. 6, pp. 535–551, 2007.

[31] O. Sigmund, "Design of multiphysics actuators using topology optimization – Part II: Two-material structures," *Computer Methods in Applied Mechanics and Engineering*, vol. 190, no. 49–50, pp. 6605–6627, Oct. 2001.

[32] L. Yin and G. K. Ananthasuresh, "Topology optimization of compliant mechanisms with multiple materials using a peak function material interpolation scheme," *Struct Multidisc Optim*, vol. 23, no. 1, pp. 49–62, Dec. 2001.

[33] S. H. Jeong, D.-H. Choi, and G. H. Yoon, "Separable stress interpolation scheme for stress-based topology

optimization with multiple homogenous materials," *Finite Elements in Analysis and Design*, vol. 82, pp. 16–31, May 2014.
[34] L. P. Chaves and J. Cunha, "Design of carbon fiber reinforcement of concrete slabs using topology optimization," *Construction and Building Materials*, vol. 73, pp. 688–698, Dec. 2014.
[35] N. de Kruijf, S. Zhou, Q. Li, and Y.-W. Mai, "Topological design of structures and composite materials with multiobjectives," *International Journal of Solids and Structures*, vol. 44, pp. 7092–7109, 2007.
[36] J. P. Blasques and M. Stolpe, "Multi-material topology optimization of laminated composite beam cross sections," *Composite Structures*, vol. 94, no. 11, pp. 3278–3289, Nov. 2012.
[37] J. Park and A. Sutradhar, "A multi-resolution method for 3D multi-material topology optimization," *Computer Methods in Applied Mechanics and Engineering*, Nov. 2014.
[38] M. Y. Wang and X. Wang, "'Color' level sets: a multi-phase method for structural topology optimization with multiple materials," *Computer Methods in Applied Mechanics and Engineering*, vol. 193, no. 6–8, pp. 469–496, Feb. 2004.
[39] M. Y. Wang, S. Chen, X. Wang, and Y. Mei, "Design of Multimaterial Compliant Mechanisms Using Level-Set Methods," *J. Mech. Des.*, vol. 127, no. 5, pp. 941–956, Jan. 2005.
[40] X. Wang, Y. Mei, and M. Y. Wang, "Level-set method for design of multi-phase elastic and thermoelastic materials," *Int J Mech Mater Des*, vol. 1, no. 3, pp. 213–239, Sep. 2004.
[41] G. Michailidis, G. Delgado, C. Dapogny, and G. Allaire, "Multi-phase structural optimization via a level set method," report, 2013.
[42] N. Vermaak, G. Michailidis, G. Parry, R. Estevez, G. Allaire, and Y. Bréchet, "Material interface effects on the topology optimization of multi-phase structures using a level set method," *Struct Multidisc Optim*, pp. 1–22, Jun. 2014.
[43] M. Y. Wang and S. Zhou, "Synthesis of shape and topology of multi-material structures with a phase-field method," *J Computer-Aided Mater Des*, vol. 11, no. 2–3, pp. 117–138, Jun. 2005.
[44] Y. Wang, Z. Luo, Z. Kang, and N. Zhang, "A multi-material level set-based topology and shape optimization method," *Computer Methods in Applied Mechanics and Engineering*, vol. 283, no. 1, pp. 1570–1586, 2015.
[45] Y. M. Xie and G. P. Steven, "A simple evolutionary procedure for structural optimization," *Computers & Structures*, vol. 49, no. 5, pp. 885–896, Dec. 1993.
[46] D. N. Chu, Y. M. Xie, A. Hira, and G. P. Steven, "Evolutionary structural optimization for problems with stiffness constraints," *Finite Elements in Analysis and Design*, vol. 21, no. 4, pp. 239–251, Apr. 1996.
[47] O.M. Querin, G.P. Steven, and Y.M. Xie, "Evolutionary structural optimisation (ESO) using a bidirectional algorithm," *Engineering Computations*, vol. 15, no. 8, pp. 1031–1048, Dec. 1998.
[48] O. M. Querin, G. P. Steven, and Y. M. Xie, "Evolutionary structural optimisation using an additive algorithm," *Finite Elements in Analysis and Design*, vol. 34, no. 3–4, pp. 291–308, Feb. 2000.
[49] X. Liu, W.-J. Yi, Q. S. Li, and P.-S. Shen, "Genetic evolutionary structural optimization," *Journal of Constructional Steel Research*, vol. 64, no. 3, pp. 305–311, Mar. 2008.
[50] O. Sigmund, "On the usefulness of non-gradient approaches in topology optimization," *Structural and Multidisciplinary Optimization*, vol. 43, pp. 589–596, 2011.
[51] A. Ramani, "A pseudo-sensitivity based discrete variable approach to structural topology optimization with multiple materials," *Structural and Multidisciplinary Optimization*, vol. 41, pp. 913–934, 2009.
[52] A. Ramani, "Multi-material topology optimization with strength constraints," *Structural and Multidisciplinary Optimization*, vol. 43, pp. 597–615, 2011.
[53] A. A. Novotny, "Topological-Shape Sensitivity Method: Theory and Applications," *Solid Mechanics and its Applications*, vol. 137, pp. 469–478, 2006.
[54] K. Suresh and M. Takalloozadeh, "Stress-Constrained Topology Optimization: A Topological Level-Set Approach," *Structural and Multidisciplinary Optimization*, vol. 48, no. 2, pp. 295–309, 2013.
[55] S. Deng and K. Suresh, "An Augmented Topological Level-Set Method for Constrained Multi-Load Topology Optimization," *Structural and Multidisciplinary Optimization*, vol. Submitted, 2014.
[56] M. Schneider and H. Andra, "The topological gradient in anisotropic elasticity with an eye towards lightweight design," *Mathematical Methods in Applied Sciences*, vol. 37, no. 11, pp. 1624–1641, 2014.
[57] G. D. Keeffe, "Optimization of composite structures: A shape and topology sensitivity analysis," Ph.D., Ecole Polytechnique, Universite Paris-Saclay, 1014.
[58] T. Gao and W. Zhang, "A mass constraint formulation for structural topology optimization with multiphase materials," *International Journal for Numerical Methods in Engineering*, vol. 88, no. 8, pp. 774–796, Nov. 2011.
[59] S. Amstutz, "Connections between topological sensitivity analysis and material interpolation schemes in topology optimization," *Structural and Multidisciplinary Optimization*, vol. 43, pp. 755–765, 2011.
[60] K. K. Choi and N. H. Kim, *Structural Sensitivity Analysis and Optimization I: Linear Systems*. New York: Springer, 2005.
[61] T. J. R. Hughes, I. Levit, and J. Winget, "An element-by-element solution algorithm for problems of structural and solid mechanics," *Comput Meth Appl Mech Eng*, vol. 36, no. 2, pp. 241–254, 1983.
[62] P. Yadav and K. Suresh, "Large Scale Finite Element Analysis Via Assembly-Free Deflated Conjugate Gradient," *J. Comput. Inf. Sci. Eng*, vol. 14, no. 4, pp. 041008–1: 041008–9, 2014.
[63] K. Suresh and P. Yadav, "Large-Scale Modal Analysis on Multi-Core Architectures," in *Proceedings of the ASME 2012 International Design Engineering Technical*

Conferences & Computers and Information in Engineering Conference, Chicago, IL, 2012.
[64] Y. Saad, M. Yeung, J. Erhel, and F. Guyomarc'h, "A Deflated Version of the Conjugate Gradient Algorithm," *SIAM Journal on Scientific Computing*, vol. 21, no. 5, pp. 1909–1926, 2000.
[65] O. Sigmund, "Morphology-based black and white filters for topology optimization," *Structural and Multidisciplinary Optimization*, vol. 33, pp. 401–424, 2007.